HHS Public Access

Author manuscript

Dev Dyn. Author manuscript; available in PMC 2022 February 01.

Published in final edited form as:

Dev Dyn. 2021 February ; 250(2): 263–273. doi:10.1002/dvdy.252.

Phosphosite T674A mutation in kinesin family member 3A fails to reproduce tissue and ciliary defects characteristic of CILK1 loss of function

Casey D. Gailey[1], **Eric J. Wang**[1], **Li Jin**[2], **Sean Ahmadi**[1], **David L. Brautigan**[3,4], **Xudong Li**[2], **Wenhao Xu**[3], **Michael M. Scott**[1], **Zheng Fu**[1,4]

[1]Department of Pharmacology, University of Virginia School of Medicine, Charlottesville, Virginia

[2]Department of Orthopedic Surgery, University of Virginia School of Medicine, Charlottesville, Virginia

[3]Department of Microbiology, Immunology, and Cancer Biology, University of Virginia School of Medicine, Charlottesville, Virginia

[4]NCI designated Cancer Center, Cancer Biology Program, University of Virginia School of Medicine, Charlottesville, Virginia

Abstract

Background: Kinesin family member 3A (KIF3A) is a molecular motor protein in the heterotrimeric kinesin-2 complex that drives anterograde intraflagellar transport. This process plays a pivotal role in both biogenesis and maintenance of the primary cilium that supports tissue development. Ciliogenesis associated kinase 1 (CILK1) phosphorylates human KIF3A at Thr672. CILK1 loss of function causes ciliopathies that manifest profound and multiplex developmental defects, including hydrocephalus, polydactyly, shortened and hypoplastic bones and alveoli airspace deficiency, leading to perinatal lethality. Prior studies have raised the hypothesis that CILK1 phosphorylation of KIF3A is critical for its regulation of organ development.

Results: We produced a mouse model with phosphorylation site Thr674 in mouse Kif3a mutated to Ala. Kif3a T674A homozygotes are viable and exhibit no skeletal and brain abnormalities, and only mildly reduced airspace in alveoli. Mouse embryonic fibroblasts carrying Kif3a T674A mutation show a normal rate of ciliation and a moderate increase in cilia length.

Correspondence: Zheng Fu, Department of Pharmacology, University of Virginia School of Medicine, Charlottesville, Virginia. zf6n@virginia.edu.

AUTHOR CONTRIBUTIONS

Casey Gailey: Data curation; formal analysis; investigation; methodology; software; validation; visualization; writing-original draft. **Eric Wang:** Data curation; formal analysis; investigation; methodology; software; validation. **Li Jin:** Data curation; formal analysis; funding acquisition; investigation; methodology; project administration; resources; supervision; validation; visualization; writing-original draft. **Sean Ahmadi:** Data curation; formal analysis; investigation; methodology; software; validation; visualization. **David Brautigan:** Conceptualization; formal analysis; funding acquisition; investigation; project administration; resources; supervision; writing-review and editing. **Xudong Li:** Funding acquisition; investigation; project administration; resources; supervision. **Wenhao Xu:** Formal analysis; funding acquisition; investigation; methodology; resources; supervision; validation; writing-original draft. **Michael Scott:** Formal analysis; funding acquisition; investigation; methodology; resources; supervision; validation. **Zheng Fu:** Conceptualization; data curation; formal analysis; funding acquisition; investigation; methodology; project administration; resources; software; supervision; validation; visualization; writing-original draft; writing-review and editing.

CONFLICT OF INTEREST

The authors declare no conflict of interest.

Conclusion: These results indicate that eliminating Kif3a Thr674 phosphorylation by Cilk1 is insufficient to reproduce the severe developmental defects in ciliopathies caused by Cilk1 loss of function. This suggests KIF3A-Thr672 phosphorylation by CILK1 is not essential for tissue development and other substrates are involved in CILK1 ciliopathies.

Keywords

ciliogenesis; ciliopathy; development; kinase; primary cilia

1 | INTRODUCTION

Most eukaryotic cells use the primary cilium as the sensory organelle and signaling antenna to detect environmental cues and transmit extracellular signals to modulate intracellular processes and cell behaviors.[1] Primary cilia are enriched with membrane receptors, ion channels, metabolic enzymes, and second messengers, and provide a highly efficient and intricate infrastructure for the operation of many signaling pathways such as Hedgehog, G protein-coupled receptors (GPCR), and receptor tyrosine kinases (RTK).[2,3] A variety of human genetic disorders, collectively called ciliopathies, is caused by mutations in ciliary proteins that disrupt the integrity of cilia structure and signaling.[4] A deeper comprehension of the molecular mechanism regulating cilia structure and function will be instrumental for a better understanding of the pathogenesis of ciliopathies.

Ciliogenesis associated kinase 1 (CILK1),[5] formerly known as intestinal cell kinase (ICK),[6] is emerging as a key protein localized at the cilia base that restricts cilia biogenesis and length.[7–13] Human mutations in *CILK1* have been linked to ciliopathies and epilepsy.[10,14–16] Both Cilk1 null and mutated (R272Q) knock-in mouse models have shown that CILK1 dysfunction causes perinatal lethality and detrimental effects on multi-organ development, resulting in anomalies such as hydrocephalus, alveoli airspace deficiency, polydactyly, shortened and hypoplastic bones.[7,8,10,11,17] Although the essential role for CILK1 in development and primary cilia has been established, we still do not know much about which CILK1 substrates mediate its actions on developmental and ciliary phenotype. Among several candidate substrates identified for CILK1, kinesin family member 3A (KIF3A) has gained significant attention because its critical role as a motor protein in ciliary transport is directly related to the control of cilia formation.[7,12]

Intraflagellar transport (IFT) along cilia axonemal microtubules consists of kinesin-mediated anterograde and dynein-mediated retrograde transport. Kinesin 3A/3B dimeric motor subunits and kinesin-associated protein (KAP) form the heterotrimeric Kinesin-2 complex.[18] Anterograde IFT mediated by KIF3A/KIF3B/KAP is essential for the assembly and maintenance of primary cilia.[19,20] The C-terminal cargo-binding domain of human KIF3A contains multiple phosphorylation sites, including PKA site Ser687, CaMKII sites Thr692 and Ser696, and CILK1 site Thr672. Phosphorylation of S687/T692/S696 enhances the cargo-binding and trafficking activities of KIF3A.[21] The CILK1 site Thr672 in human KIF3A is highly conserved among metazoans. CILK1 robustly phosphorylates human KIF3A-Thr672 (mouse Kif3a-Thr674) in vitro and in vivo.[7,12] A previous study indicates that mouse Kif3a-T674A mutant protein has a stronger capability than Kif3a-WT protein

to rescue cilia formation in Kif3a-knockdown cells, suggesting a restrictive effect of Kif3a-Thr674 phosphorylation on cilia assembly.[7] Based on these pieces of evidence, we postulated that phosphorylation of KIF3A-Thr672 acts as an important downstream effector through which CILK1 restricts cilia assembly and regulates organ development. To test this hypothesis, we generated a Kif3a-T674A knock-in mouse model and interrogated the developmental and ciliary phenotype caused by phospho-Thr674 deficiency in Kif3a.

2 | RESULTS

2.1 | Developmental phenotype of Kif3a T674A knock-in mice

We used CRISPR/Cas9 to genetically engineer several mutations in exon 17 of mouse *Kif3a* (Figure 1A). These knock-in mutations enable not only the conversion of Thr674 to Ala but also the introduction of a StuI restriction enzyme recognition site near the T674A mutation, as confirmed by sequencing results (Figure 1B). Restriction digestion of PCR products by StuI allowed us to distinguish between *Kif3a* wild type (WT) and mutant alleles, as shown in genotyping results (Figure 1C). We then evaluated whether this mutation affects Kif3a protein stability, Thr-674 phosphorylation and subcellular localization in mouse embryonic fibroblasts. While similar levels of Kif3a WT and T674A mutant proteins were detected in Kif3a immunoprecipitates, Kif3a-T674 phosphorylation was completely abolished in Kif3a T674A homozygous mutant proteins and markedly reduced in Kif3a T674A heterozygous mutant proteins (Figure 2A). These results suggest the T674A mutation eliminated T674 phosphorylation but did not alter Kif3a stability. Kif3a WT protein was enriched in the perinuclear region, showing punctate staining in a reticular pattern (Figure 2B). A fraction of Kif3a resided at the base of the primary cilium (Figure 2B'). Kif3a T674A mutant protein did not appear to be mislocalized (Figure 2C–C', 2D–D'); there was not a distinct difference between Kif3a mutant and WT proteins in their subcellular distribution (Figure 2B–D).

Mice bearing Cilk1 homozygous null or kinase deficient (R272Q) mutations died at birth and showed profound developmental abnormalities in multi-organ systems.[7,8,10,11,17] The perinatal lethality phenotype of these Cilk1 mutant mice was linked to severe alveolar airspace deficiency in the lung.[11] In contrast, mice bearing Kif3a T674A mutations were viable with normal lung/body weight ratio (Figure 3A). Compared with wild type lungs, Kif3a homozygous, but not heterozygous, mutant lungs showed only a moderate decrease in alveolar airspace (Figure 3B–E). Cilk1 homozygous mutant mice also displayed extensive skeletal defects, including polydactyly, shortened limbs, and deformed spine.[10,17] However, these aberrations were not observed in whole-mount skeletal staining (Figure 4A–B) and full-body X-Ray scans (Figure 4C–D) of Kif3a T674A mutant mice. It is worthy to note that minor differences present, such as ectopic processes and increased ossification in digits (Figure 4A), were not consistent among multiple animals.

Ciliopathy patients carrying *CILK1* mutations displayed ventricular hydrocephalus and absence of third ventricle.[14] Cilk1 null mice showed dilated ventricles and smaller cerebellum and hippocampal dentate gyrus (DG).[7,8] Compared with wild type mice, Kif3a mutant mice have similar brain/body weight ratios (Figure 5A). By contrast to Cilk1 mutant brains, Kif3a mutant brains showed neither reduction in the size of cerebellum (Figure 5B) and hippocampal DG (Figure 5C–D) nor dilation of lateral ventricles or absence of third

ventricle (Figure 5E–F). We concluded that absence of Kif3a phosphorylation at Thr674 produced only mild airspace deficiency in the lung and was insufficient to reproduce the profound anomalies in the skeleton and the brain caused by Cilk1 loss of function.

2.2 | Cilia phenotype of Kif3a T674A knock-in cells

We investigated the impact of this phosphosite mutation in Kif3a on cilia length and formation. We isolated mouse embryonic fibroblasts (MEFs) from Kif3a WT and T674A mutant embryos. We immunostained MEFs with cilia marker Arl13B, calculated percent of ciliated cells and then measured cilia length. Our results indicate that about 60% of wild type MEF cells were ciliated under normal growth conditions, and the average cilia length was 3.7 μm (Figures 6, 7). By comparison, MEFs bearing Kif3a homozygous T674A mutation showed an insignificant change in percent of ciliation but an 8% increase in average cilia length (Figures 6, 7). MEFs bearing Kif3a heterozygous T674A mutation, however, were not significantly different from WT MEFs in cilia number and cilia length.

We immunostained MEFs to examine distribution patterns of three ciliary proteins: intraflagellar transport protein 88 (IFT88), adenylate cyclase 3 (AC3), and GLI family zinc finger protein 2 (GLI2). IFT88 showed two basic ciliary distribution patterns: enrichment at the base and along the axoneme, and enrichment at the base and the tip (Figure 8A). This localization pattern of IFT88 was not significantly altered by Kif3a T674A mutation (Figure 8A–B). Both AC3 and GLI2 were distributed along the entire axoneme of the cilium, showing no obvious enrichment at the base or the tip (Figure 8C–D). Like IFT88, the ciliary localization patterns of AC3 and GLI2 were not considerably different between Kif3a WT and T674A mutant cells (Figure 8C–D). These data indicate that although Kif3a T674A mutant cilium was slightly longer, the distribution of selected ciliary proteins was not grossly different from that in wild type cilia.

Cilia elongation caused by Cilk1 loss-of-function mutations is associated with alterations in Hedgehog (Hh) signaling and autophagy.[11] We thus examined the expression levels of Hh-responsive transcription factor GLI2 and autophagosome marker LC3B (microtubule-associated protein 1 light chain 3 beta) by Western blotting. MEFs carrying Kif3a T674A homozygous mutations showed a modest increase in GLI2 and LC3B signals compared with wild type MEFs (Figure 8E). However, there were no noticeable differences in the levels of autophagy substrates SQSTM1 (Sequestosome-1) and OFD1 (oral-facial-digital syndrome 1) between Kif3a mutant and wild type cells (Figure 8E). These data suggest that Kif3a T674A mutation produced only a mild impact on Hh signaling and autophagy.

3 | DISCUSSION

By knocking-in a mutation at Thr-674 in Kif3a that prevents phosphorylation by Cilk1 at this site, our study addresses whether, and to what extent, disruption of phosphorylation of a specific substrate of CILK1 can recapitulate the profound developmental and ciliary phenotypes of ciliopathies linked to CILK1 loss of function. Our results demonstrate that without phosphorylation of Kif3a at Thr674 there is only a mild impact on the primary cilia and tissue development. This suggests that CILK1 requires other substrates in addition to KIF3A to control ciliary structure and function and tissue development.

While inactivating mutations of Cilk1 cause significant reduction of cilia number and change in cilia length, the Kif3a T674A mutation produces only moderate effects on cilia length and no change in cilia number in MEFs. This disparity in phenotypes between Cilk1 and Kif3a mutants suggests that phosphorylation of Kif3a-Thr674 plays a limited role in Cilk1 regulation of cilia. Our results here underscore the importance of testing other candidate substrates of CILK1, such as Scythe and mTORC1,[22–24] for their individual and synergistic contributions to the control of cilia assembly and maintenance.

Lung and cilia phenotypes were only detected in mice and MEFs carrying both *Kif3a* T674A mutant alleles, indicating that the phosphosite-deficient mutation T674A in *Kif3a* is recessive. *Cilk1* null or R272Q mutations are also recessive in producing ciliopathy phenotypes. These results together suggest that the functional allele of *Cilk1* or *Kif3a* is haplosufficient to contribute to the maintenance of cilia length and alveolar airspace.

Our findings add new insights into the role of KIF3A C-terminal phosphorylation in the control of cilia biogenesis and cilia length. Phosphorylation of S687/T692/S696 in KIF3A C-terminus enhances cargo-binding and transport activities, based on changes due to mutation of all three sites.[21] In contrast, our data showing that lack of Kif3a phosphorylation at Thr674 induces longer cilia implicates an inhibitory effect of Kif3a phosphorylation on cilia growth. Do these nearby phosphosites in KIF3A C-terminus have synergistic or opposing effects on cilia? How these multiple sites coordinately regulate cilia transport, structure, and function under both physiological and pathological conditions? These questions merit further consideration and experimentation.

Our analyses of cilia and developmental phenotypes associated with Kif3a T674A mutation were not exhaustive and have several limitations. First, we have not determined whether the ciliary phenotype of Kif3a T674A mutant is present in cells other than MEFs. Knowledge about regulation of this specific phosphorylation event in a cell type- and developmental stage- specific manner must be gained to guide more indepth phenotypic analyses in our future studies. Second, it remains to be determined if Kif3a T674A mutation affects cilia turnover rate in cells to impact various cellular and developmental processes. The cilium is a dynamic structure.[25–27] Cilia turnover is intrinsically linked to cell cycle progression and cell growth conditions such as starvation and hypoxia.[28–30] Alterations of ciliary dynamics under pathological conditions can influence cell fate choices and tissue homeostasis.[31] Third, we have not determined the impact of Kif3a T674A mutation on organ systems other than lung, skeleton, and brain. Ciliopathies affect multi-organ systems. In this study, we focused our analyses on three organs that were profoundly affected by Cilk1 mutations.[11,14] However, it is possible that Kif3a T674A mutation may have a more pronounced impact on other organs such as endocrine glands, which are also common targets of ciliopathic mutations.[14,32] Fourth, mouse mutants lacking Kif3a exhibited ciliary morphogenesis defects, randomized left–right asymmetry, and numerous structural abnormalities[33,34]; thus it would be very interesting to determine what cellular and developmental phenotypes of Kif3a null mice can be rescued by Kif3a T674A mutant. These topics constitute the lines of our further investigation about the functional impact of CILK1 phosphorylation of KIF3A.

The precise mechanism underpinning the regulation of cilia length and alveolar space by Kif3a-Thr674 phosphorylation is unclear. Although our study did not reveal any gross mislocalization of several ciliary proteins, more detailed and quantitative analyses are required to provide definitive evidence showing the impact of Kif3a-Thr674 phosphorylation on ciliary transport. Our data from MEFs indicate that only moderate changes in the expression of Hh signaling and autophagy markers were associated with slightly longer cilia in Kif3a T674A mutants. Whether and to what extent this cilia length alteration can impact ciliary signaling and autophagy in lung cells and affect alveolar structure merits further investigation. To follow up on our phenotypic analysis presented here, we will continue to investigate several possible mechanisms that may link this phosphorylation event to the regulation of cilia transport and cilia length, including any potential effects on KIF3A interactions with KIF3B and KAP in the Kinesin-2 complex, KIF3A motor activity, and KIF3A cargo-binding ability.

4 | EXPERIMENTAL PROCEDURES

4.1 | Kif3a T674A knock-in mouse strain

All procedures involving animals were performed in accordance with ethical standards in an animal protocol that was approved by the Institutional Animal Care and Use Committee. The CRISPR-assisted technology was used to generate the Kif3a T674A knock-in mouse. A sgRNA (Figure 1A) is selected based on the search via the CRISPR guide design algorithm CRISPOR http://crispor.tefor.net/. The T674A (ACC > GCA) point mutation and a silent mutation (CCA > CCT) for creating a StuI restriction cutting site near the T674A mutation were introduced into the exon 17 of the wild-type *Kif3a* allele to generate *Kif3a*/T674A repair template (ssODN). Reagents crRNA, tracrRNA, Cas9 and ssODN were purchased from IDT (Coralville, IA). Reagents crRNA and tracrRNA were diluted to 1 μg/μl in RNase-free microinjection buffer (10 mM of Tris-HCl, pH 7.4, 0.25 mM of EDTA). 5 μL crRNA and 10 μL tracrRNA were mixed and annealed in a thermocycler by heating the mixture to 95°C for 5 minutes and ramped down to 25°C at 5°C/min. Ribonucleic protein (RNP) complex was formed by mixing and incubating Cas9 at 0.5 μg/μl with crRNA/tracrRNA at 0.15 μg/μl in RNase-free microinjection buffer at 37°C for 10 minutes. Reagent ssODN containing the desired amino acid substitutions was added at 0.5 μg/μl concentration. Fertilized eggs were collected from B6SJLF1 females mated with males. RNP and ssODN were co-delivered into fertilized eggs by electroporation with BioRad Gene Pulser electroporator (six pulses at 30 V for 3 msec, separated by a 100 msec interval). The zapped zygotes were cultured overnight in KSOM medium (EMD Millipore, Billerica, MA) at 37°C in 5% CO2. The next morning, zygotes that had reached the two-cell stage were implanted into the oviducts of pseudo pregnant foster mothers of ICR strain (Envigo, Indianapolis, IN). Pups born to the foster mothers were screened using tail snip DNA by PCR genotyping and restriction digestion analysis followed by Sanger's sequencing. Germline transmission of the desired alleles was confirmed by breeding the founders with wild type C57BL/6J mice. Animals were housed in a temperature-controlled colony room on a 12- hour light cycle, and had access to food and water ad libitum. Aging breeder mice were euthanized by CO_2 inhalation. Experimental mice were euthanized by cervical dislocation before tissue harvest for histological and morphometric analysis.

4.2 | Histology and morphometric analysis

Lung tissues were isolated from young adult mice of approximately 4 weeks old for morphometric analysis. Lungs were extracted, fixed, and embedded as previously described.[11] Whole lung cross sections were mounted and stained with H&E (Hematoxylin and Eosin) for histological analysis. An Aperio ImageScope Slide Scanning Microscope (Leica Biosystems, Wetziar, Germany) was used to process the stained tissues and Fiji/ImageJ (version 1.52 t) was used to process and analyze the alveolar air space of WT and Kif3a T674A mutant lungs. Each lung was separated into smaller fields wherein the images were prepared for analysis by removing field areas of nonlung regions, blood vessels, and bronchioles so that only the alveolar-associated air space and lung tissue were quantified. These were then converted into binary images in ImageJ so that area of the tissue and air space could be separately quantified.

Limb bones were dissected from mice of postnatal day 2 for morphometric analysis. Bones were rinsed with PBS and then fixed in 95% ethanol for 2 days, followed by acetone overnight at room temperature. Limbs were stained with 0.03% Alcian blue solution, washed with two changes of 70% ethanol, and incubated with 95% ethanol overnight. Limbs were then incubated with 1% KOH for 1 hour to preclear tissues and stained with 0.005% Alizarin red solution for 4 hours. Cartilages were stained with Alcian Blue and bones were stained with Alizarin Red. After clearing, samples were placed in 100% glycerol for long-term storage and imaging (Olympus SZX12, Olympus).

Brains were dissected from mice of approximately 4 weeks old after perfusion with 4% paraformaldehyde (PFA) in 1x PBS. Isolated brains were further fixed in 4% PFA overnight, rinsed in PBS, and then paraffin embedded. Coronal sections (5 μm) were mounted and stained with H&E for histological analysis.

4.3 | Cell culture and Western blot

Mouse embryonic fibroblast (MEF) cells were isolated from Kif3a wild type and T674A mutant embryos (E14.5-E15.5) and maintained at 37°C and 5% CO_2 in Dulbecco's modified Eagle's medium supplemented with 10% fetal bovine serum, nonessential amino acids, and penicillin-streptomycin using a standard protocol.[35]

MEF cells were lysed in lysis buffer (50 mM Tris-HCl, pH 7.4, 150 mM NaCl, 1% NP-40, 2 mM EGTA, and complete protease and phosphatase inhibitors from Roche, Basel, Switzerland). Cell lysate was cleared by centrifugation. Protein extracts were boiled for 5 minutes in an equal volume of 2X Laemmli sample buffer (120 mM Tris-HCl, pH 6.8, 4% SDS, 20% glycerol, 10% β-mercaptoethanol, 0.02% bromophenol blue) and loaded on an SDS-gel. Samples were transferred to a PVDF membrane and blocked for 1 hour in 5% dry milk before incubation with primary antibodies in TBS containing 0.1% Tween-20 and 5% bovine serum albumin (BSA) for overnight at 4°C. This was followed by extensive rinses and one-hour incubation with horseradish peroxidase (HRP)-conjugated secondary antibody. Chemiluminescent signals were developed using Millipore Immobilon ECL reagents (EMD Millipore).

The following primary antibodies were used for Western blotting: KIF3A (D7G3) rabbit monoclonal antibody (Cell Signaling Technology, Danvers, MA, #8507); KIF3A phospho-Thr672 rabbit polyclonal antibody[12,13] (GenScript, Piscataway, NJ); SQSTM1 (D-3) mouse monoclonal antibody (Santa Cruz, Dallas, TX, sc-28 359); LC3B (D11) rabbit monoclonal (#3868) and β-Actin (D6A8) rabbit monoclonal (#8457) antibodies (Cell Signaling Technology, Danvers, MA); IFT88 rabbit polyclonal antibody (Proteintech, Rosemont, IL, 13967-1-AP); Gli2 rabbit polyclonal antibody (GTX46056) and OFD1 rabbit polyclonal antibody (GTX110010) (GeneTex, Irvine, California).

4.4 | Confocal immunofluorescence microcopy and cilia analysis

Mouse embryonic fibroblast (MEF) cells were grown on gelatin-coated coverslips were fixed by 4% paraformaldehyde (PFA) in PBS, rinsed in PBS, and then permeabilized by 0.2% Triton X-100 in PBS. After 1 hour in blocking buffer (3% goat serum, 0.2% Triton X-100 in PBS), cover slips were incubated in primary antibody at 4°C overnight followed by rinses in PBS and 1 hour incubation with goat anti-mouse IgG (Alexa Fluor 647-conjugated) secondary antibody (Abcam, Cambridge, MA, ab150115) and/or goat anti-rabbit IgG (Alexa Fluor 594-conjugated) secondary antibody (Abcam, Cambridge, MA, ab150084). MEF cells on cover slips were incubated with cilia marker Arl13B rabbit antibody (ProteinTech, Rosemont, IL, 17711-1-AP) for analysis of cilia length and prevalence. For localization analysis of ciliary proteins, additional cover slips were coincubated with acetylated tubulin (Lys40) mouse monoclonal antibody (ProteinTech, Rosemont, IL, 66200-1) as well as with KIF3A (D7G3) rabbit monoclonal (Cell Signaling Technology, Danvers, MA, #8507), IFT88 rabbit polyclonal (ProteinTech, Rosemont, IL, 13967-1-AP), ADCY3 rabbit polyclonal (ProteinTech, Rosemont, IL, 19492-1-AP), or Gli2 rabbit polyclonal antibody (GeneTex, Irvine, CA, GTX46056). After extensive rinses, slides were mounted in antifade reagent containing DAPI (4′, 6-diamidino-2-phenylindole) for imaging via ZEISS LSM 700 confocal microscope.

Zen 2009 program was used with the confocal Laser Scanning Microscope 700 (LSM 700) to collect z stacks at 0.5 μm intervals to incorporate the full axoneme based on cilia marker Arl13b staining. All cilia were then measured in Fiji/ImageJ (version 1.52 t) via a standardized method based on the Pythagorean Theorem in which cilia length was based on the Equation L2 = z2 + c2, in which “c” is the longest flat length measured of the z slices and “z” is the number of z slices in which the measured cilia was present multiplied by the z stack interval (0.5 μm). Z stacks were used to measure cilia lengths as described, the number of ciliated cells, as well as for qualitative analysis of localization patterns of Ift88, Adcy3, Gli2, and Kif3a.

4.5 | Statistical analysis

Quantified experimental data between different genotypes were analyzed and compared by an unpaired, two tailed Student *t*-test. Data were reported as average ± SD (SD). *P* values less than .05 were considered as significant.

ACKNOWLEDGEMENTS

Zheng Fu and David L. Brautigan conceived the project. Wenhao Xu, Zheng Fu, Eric J. Wang designed, constructed, and evaluated the mouse model. Casey D. Gailey, Eric J. Wang, Li Jin, Sean Ahmadi, Zheng Fu, David L. Brautigan, Xudong Li, Michael M. Scott performed experiments and conducted data curation and analysis. Zheng Fu, David L. Brautigan, Li Jin, Xudong Li, and Michael M. Scott contributed essential reagents/tools and acquired funding support. Zheng Fu, Casey D. Gailey, Wenhao Xu, and Li Jin contributed to the original writing, David L. Brautigan contributed to the editing of the manuscript.

We thank our colleagues at UVA Genetically Engineered Murine Model Core, Research Histology Core, and Advanced Microscopy Facility for technical support. This work was supported by National Institute of General Medical Sciences grant GM127690 to Zheng Fu, NIAMS grant AR064792 to Xudong Li, NIMH grant MH116694 to Michael M. Scott, NCI CCSG 5P30CA044579 to UVA School of Medicine research cores, University of Virginia Harrison undergraduate research grant to Eric J. Wang, and the F. Palmer Weber endowed professorship to David L. Brautigan

Funding information

National Cancer Institute, Grant/Award Number: P30CA044579; National Institute of Arthritis and Musculoskeletal and Skin Diseases, Grant/Award Number: AR064792; National Institute of General Medical Sciences, Grant/Award Number: GM127690; National Institute of Mental Health, Grant/Award Number: MH116694

Abbreviations:

ADCY3	adenylate cyclase 3
CILK1	ciliogenesis associated kinase 1
GLI2	GLI family zinc finger protein 2
ICK	intestinal cell kinase
IFT	intraflagellar transport
KIF3A/3B	kinesin family member 3A/3B
KAP	kinesin associated protein
IFT88	intraflagellar transport 88
LC3B	microtubule-associated protein 1 light chain 3 beta
MEF	mouse embryonic fibroblast
OFD1	oral-facial-digital syndrome 1
SQSTM1	sequestosome-1

REFERENCES

1. Malicki JJ, Johnson CA. The cilium: cellular antenna and central processing unit. Trends Cell Biol2. 2017;27(2):126–140. 10.1016/j.tcb.2016.08.002. [PubMed: 27634431]
2. Gerdes JM, Davis EE, Katsanis N. The vertebrate primary cilium in development, homeostasis, and disease. Cell. 2009;137(1):32–45. [PubMed: 19345185]
3. Christensen ST, Morthorst SK, Mogensen JB, Pedersen LB. Primary cilia and coordination of receptor tyrosine kinase (RTK) and transforming growth factor beta (TGF-beta) signaling. Cold Spring Harb Perspect Biol. 2017;9(6):1–18. 10.1101/cshperspect.a028167.

4. Reiter JF, Leroux MR. Genes and molecular pathways underpinning ciliopathies. Nat Rev Mol Cell Bio. 2017;18(9):533–547. 10.1038/nrm.2017.60. [PubMed: 28698599]
5. Fu Z, Gailey CD, Wang EJ, Brautigan DL. Ciliogenesis associated kinase 1: targets and functions in various organ systems. FEBS Lett. 2019;593:2990–3002. 10.1002/1873-3468.13600. [PubMed: 31506943]
6. Togawa K, Yan YX, Inomoto T, Slaugenhaupt S, Rustgi AK. Intestinal cell kinase (ICK) localizes to the crypt region and requires a dual phosphorylation site found in map kinases. J Cell Physiol. 2000;183(1):129–139. [PubMed: 10699974]
7. Chaya T, Omori Y, Kuwahara R, Furukawa T. ICK is essential for cell type-specific ciliogenesis and the regulation of ciliary transport. EMBO J. 2014;33(11):1227–1242. [PubMed: 24797473]
8. Moon H, Song J, Shin JO, et al.. Intestinal cell kinase, a protein associated with endocrine-cerebro-osteodysplasia syndrome, is a key regulator of cilia length and hedgehog signaling. Proc Natl Acad Sci U S A. 2014;111(23):8541–8546. 10.1073/pnas.1323161111. [PubMed: 24853502]
9. Broekhuis JR, Verhey KJ, Jansen G. Regulation of cilium length and intraflagellar transport by the RCK-kinases ICK and MOK in renal epithelial cells. PLoS One. 2014;9(9):e108470. 10.1371/journal.pone.0108470 PONE-D-14-23698 [pii]. [PubMed: 25243405]
10. Paige Taylor S, Kunova Bosakova M, Varecha M, et al.. An inactivating mutation in intestinal cell kinase, ICK, impairs hedgehog signalling and causes short rib-polydactyly syndrome. Hum Mol Genet. 2016;25(18):3998–4011. 10.1093/hmg/ddw240. [PubMed: 27466187]
11. Tong Y, Park SH, Wu D, et al.. An essential role of intestinal cell kinase in lung development is linked to the perinatal lethality of human ECO syndrome. FEBS Lett. 2017;591:1247–1257. 10.1002/1873-3468.12644. [PubMed: 28380258]
12. Oh YS, Wang EJ, Gailey CD, Brautigan DL, Allen BL, Fu Z. Ciliopathy-associated protein kinase ICK requires its non-catalytic carboxyl-terminal domain for regulation of Ciliogenesis. Cells. 2019;8(7):1–10. 10.3390/cells8070677.
13. Wang EJ, Gailey CD, Brautigan DL, Fu Z. Functional alterations in Ciliogenesis-associated kinase 1 (CILK1) that result from mutations linked to juvenile myoclonic epilepsy. Cells. 2020;9(3):1–11. 10.3390/cells9030694.
14. Lahiry P, Wang J, Robinson JF, et al.. A multiplex human syndrome implicates a key role for intestinal cell kinase in development of central nervous, skeletal, and endocrine systems. Am J Hum Genet. 2009;84(2):134–147. 10.1016/j.ajhg.2008.12.017. [PubMed: 19185282]
15. Oud MM, Bonnard C, Mans DA, et al.. A novel ICK mutation causes ciliary disruption and lethal endocrine-cerebro-osteodysplasia syndrome. Cilia. 2016;5:8. 10.1186/s13630-016-0029-1. [PubMed: 27069622]
16. Bailey JN, de Nijs L, Bai D, et al.. Variant intestinal-cell kinase in juvenile myoclonic epilepsy. N Engl J Med. 2018;378(11):1018–1028. 10.1056/NEJMoa1700175. [PubMed: 29539279]
17. Ding M, Jin L, Xie L, et al.. A murine model for human ECO syndrome reveals a critical role of intestinal cell kinase in skeletal development. Calcif Tissue Int. 2018;102(3):348–357. 10.1007/s00223-017-0355-3. [PubMed: 29098359]
18. Cole DG. Kinesin-II, coming and going. J Cell Biol. 1999;147(3):463–466. 10.1083/jcb.147.3.463. [PubMed: 10545491]
19. Engelke MF, Waas B, Kearns SE, et al.. Acute inhibition of Heterotrimeric Kinesin-2 function reveals mechanisms of Intraflagellar transport in mammalian cilia. Curr Biol. 2019;29(7):1137–1148. 10.1016/j.cub.2019.02.043. [PubMed: 30905605]
20. Ishikawa H, Marshall WF. Intraflagellar transport and Ciliary dynamics. Cold Spring Harb Perspect Biol. 2017;9(3):1–13. 10.1101/cshperspect.a021998.
21. Ichinose S, Ogawa T, Hirokawa N. Mechanism of activity-dependent cargo loading via the phosphorylation of KIF3A by PKA and CaMKIIa. Neuron. 2015;87(5):1022–1035. 10.1016/j.neuron.2015.08.008. [PubMed: 26335646]
22. Fu Z, Kim J, Vidrich A, Sturgill TW, Cohn SM. Intestinal cell kinase, a MAP kinase-related kinase, regulates proliferation and G1 cell cycle progression of intestinal epithelial cells. Am J Physiol Gastrointest Liver Physiol. 2009;297(4):G632–G640. 10.1152/ajpgi.00066.2009. [PubMed: 19696144]

23. Fu Z, Larson KA, Chitta RK, et al.. Identification of yin-yang regulators and a phosphorylation consensus for male germ cell-associated kinase (MAK)-related kinase. Mol Cell Biol. 2006;26(22):8639–8654. 10.1128/MCB.00816-06. [PubMed: 16954377]
24. Wu D, Chapman JR, Wang L, et al.. Intestinal cell kinase (ICK) promotes activation of mTOR complex 1 (mTORC1) through phosphorylation of raptor Thr-908. J Biol Chem. 2012;287(15):12510–12519. 10.1074/jbc.M111.302117. [PubMed: 22356909]
25. Hsu KS, Chuang JZ, Sung CH. The biology of Ciliary dynamics. Cold Spring Harb Perspect Biol. 2017;9(4):1–14. 10.1101/cshperspect.a027904.
26. Santos N, Reiter JF. Building it up and taking it down: the regulation of vertebrate ciliogenesis. Dev Dyn. 2008;237(8):1972–1981. 10.1002/dvdy.21540. [PubMed: 18435467]
27. Roberson EC, Tran NK, Konjikusic MJ, Fitch RD, Gray RS, Wallingford JB. A comparative study of the turnover of multiciliated cells in the mouse trachea, oviduct, and brain. Dev Dyn. 2020;249(7):898–905. 10.1002/dvdy.165. [PubMed: 32133718]
28. Izawa I, Goto H, Kasahara K, Inagaki M. Current topics of functional links between primary cilia and cell cycle. Cilia. 2015;4:12. 10.1186/s13630-015-0021-1. [PubMed: 26719793]
29. Pierce NW, Nachury MV. Cilia grow by taking a bite out of the cell. Dev Cell. 2013;27(2):126–127. 10.1016/j.devcel.2013.10.013. [PubMed: 24176638]
30. Shamloo K, Chen J, Sardar J, et al.. Chronic Hypobaric Hypoxia Modulates Primary Cilia Differently in Adult and Fetal Ovine Kidneys. Front. Physiol2017;8(677):1–11. [PubMed: 28154536]
31. Blitzer AL, Panagis L, Gusella GL, Danias J, Mlodzik M, Iomini C. Primary cilia dynamics instruct tissue patterning and repair of corneal endothelium. Proc Natl Acad Sci U S A. 2011;108(7):2819–2824. 10.1073/pnas.1016702108. [PubMed: 21285373]
32. Elliott KH, Millington G, Brugmann SA. A novel role for cilia-dependent sonic hedgehog signaling during submandibular gland development. Dev Dyn. 2018;247(6):818–831. 10.1002/dvdy.24627. [PubMed: 29532549]
33. Marszalek JR, Ruiz-Lozano P, Roberts E, Chien KR, Goldstein LS. Situs inversus and embryonic ciliary morphogenesis defects in mouse mutants lacking the KIF3A subunit of kinesin-II. Proc Natl Acad Sci U S A. 1999;96(9):5043–5048. 10.1073/pnas.96.9.5043. [PubMed: 10220415]
34. Takeda S, Yonekawa Y, Tanaka Y, Okada Y, Nonaka S, Hirokawa N. Left-right asymmetry and kinesin superfamily protein KIF3A: new insights in determination of laterality and mesoderm induction by kif3A−/− mice analysis. J Cell Biol. 1999;145(4):825–836. 10.1083/jcb.145.4.825. [PubMed: 10330409]
35. Durkin ME, Qian X, Popescu NC, Lowy DR. Isolation of mouse embryo fibroblasts. Bio Protoc. 2013;3(18). 1–5.

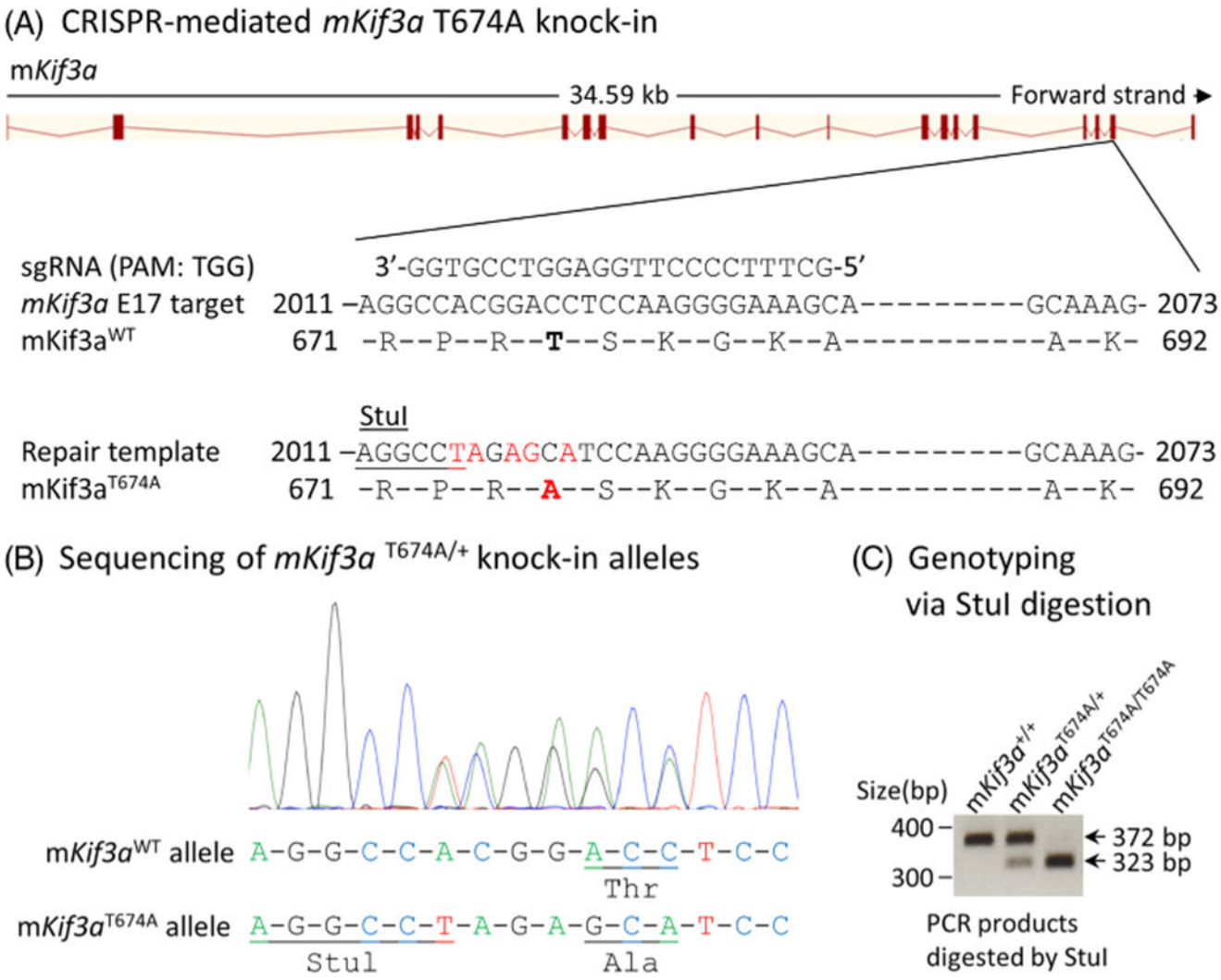

FIGURE 1.

Generation of the Kif3a T674A knock-in mouse model. A, A schematic illustration of CRISPR/Cas9-mediated knock-in of the phospho-deficient mutation T674A in mKif3a. A StuI restriction enzyme cutting site was also introduced into the *mKif3a*^{T674A} mutant allele by a silent mutation (CCA → CCT). B, Sequencing results confirming designed mutations that not only convert Thr674 to Ala but also introduce a new StuI site near T674A for genotyping. Two silent base substitutions (CGG → AGA) were also engineered to deter the recut of the repair template by Cas9 nuclease. C, Genotyping results from StuI-digested PCR products that can distinguish between *mKif3a*$^{+/+}$ (wild type), *mKif3a*$^{T674A/+}$ (heterozygotes) and *mKif3a*$^{T674A/T674A}$ (homozygotes) littermates

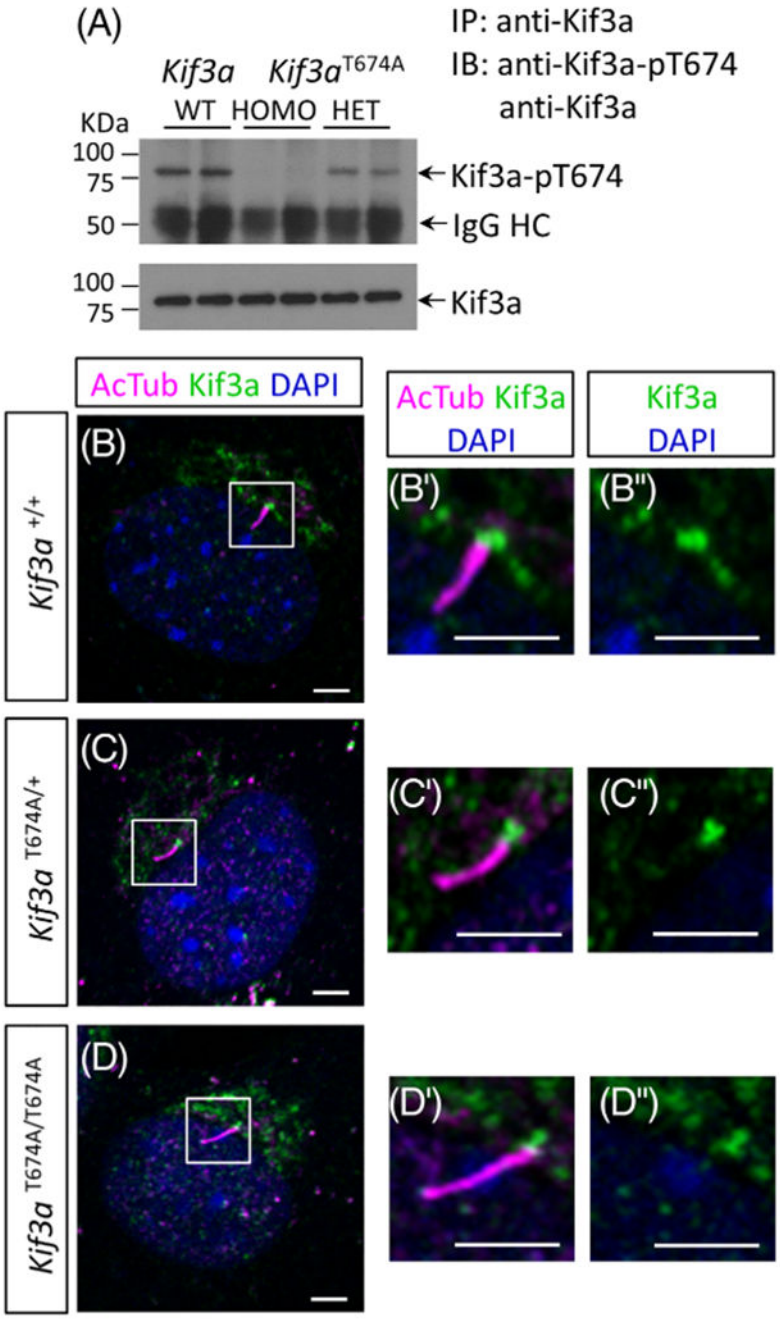

FIGURE 2.

Kif3a-Thr674 phosphorylation and Kif3a subcellular localization in Kif3a wild type and T674A mutant mouse embryonic fibroblasts. A, Kif3a was immunoprecipitated (IP) from whole cell extracts of Kif3a wild type (WT), T674A heterozygous (HET) and homozygous (HOMO) mouse embryonic fibroblasts (MEFs). Immunoblots (IB) of Kif3a IP samples show phospho-Kif3a-T674 and total Kif3a signals in Kif3a WT and T674A mutant MEFs. B-D, Confocal immunofluorescence images illustrate Kif3a (green) staining at the perinuclear region (DAPI staining for the nucleus, blue), and at the base of the primary

cilium (Arl13b staining for the primary cilium, magenta) in Kif3a WT and T674A MEFs. B'-D' and B"-D" are higher magnification images of regions within the white frame in B-D, showing triple or double immunofluorescence as indicated. Scale bar, 3 μm

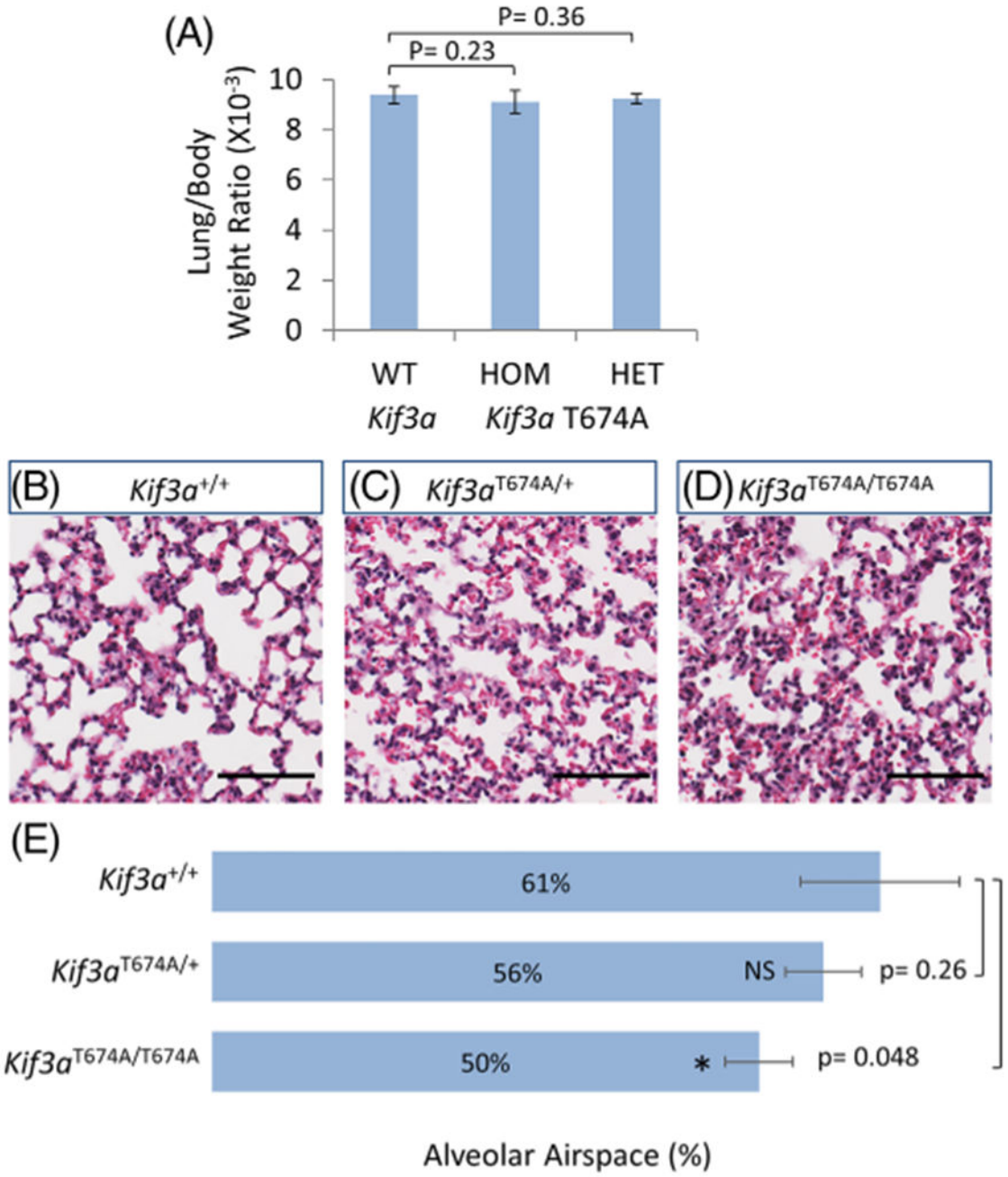

FIGURE 3.

Kif3a T674A homozygous mutant lungs exhibit mildly reduced alveolar airspace. A, Lung/body weight ratios were measured and shown for Kif3a wild type (n = 7, 4 weeks old) and T674A mutant mice (n = 7 homozygotes, 6 heterozygotes, 4 weeks old). Shown are average ± SD. B-D, H&E stained lung tissue sections of young adult Kif3a wild type and T674A mutant mice (n = 4 per genotype, 4 weeks old). Scale bar, 80 μm. E, Air sac area measurements for the entire lung tissue of young adult mice (n = 4, 4 weeks old), excluding

nonalveolar associated areas including bronchi and blood vessels. Shown are average ± SD, $*P < .05$, NS = not significant

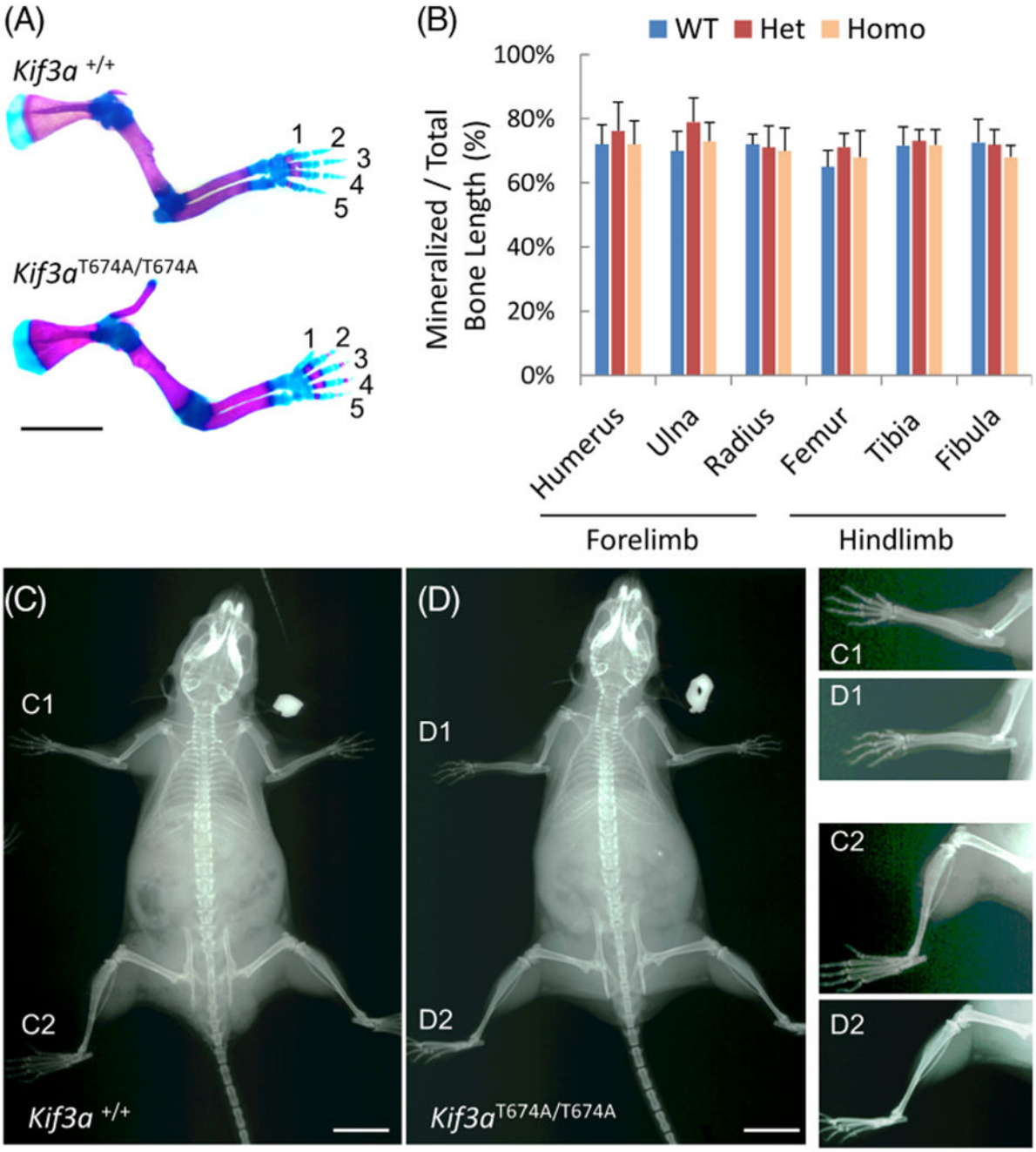

FIGURE 4.

Kif3a T674A mutant limbs exhibit normal bone and digit structure. A, Representative images of Kif3a wild type and T674A homozygote forelimb stained in Alizarin red S (calcified tissue in red) and Alcian blue (cartilage tissue in blue). Scale bar, 5 mm. B, Quantification data of bone length (mineralized bone vs total bone length) of Kif3a WT and T674A mutant littermates of postnatal day 2 (average ± SD, n = 4 mice per genotype). C-D, Representative full-body X-Ray scans of Kif3a WT and T674A homozygotes. Scale bar, 1

cm. C1-D1 and C2-D2 are blow-up images of Kif3a WT and T674 mutant forelimbs and hindlimbs, respectively

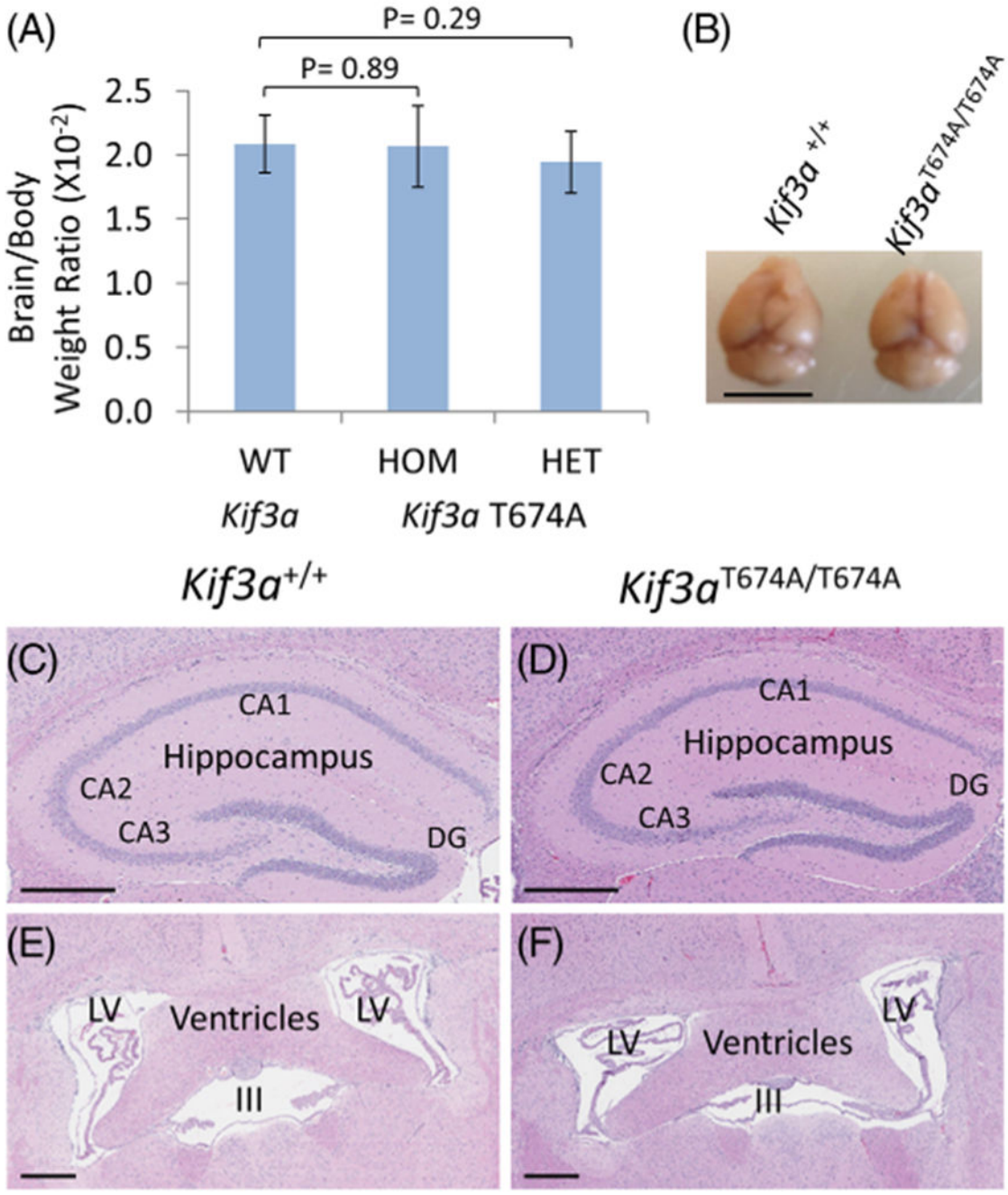

FIGURE 5.

Kif3a T674A mutant brains exhibit normal hippocampal and ventricular structure. A, brain/body weight ratios for Kif3a wild type (WT) (n = 7, 4 weeks old) and T674A mutant mice (n = 7 homozygotes, 6 heterozygotes, 4 weeks old). Shown are average ± SD. B, the dorsal view of dissected brains from Kif3a WT and T674A homozygotes, scale bar, 0.5 cm; C-F, the coronal brain sections illustrating hippocampal and ventricular structures in Kif3a WT and T674A homozygotes, scale bar, 0.5 mm. CA, Cornu Ammon; DG, Dentate Gyrus; LV, Lateral Ventricle

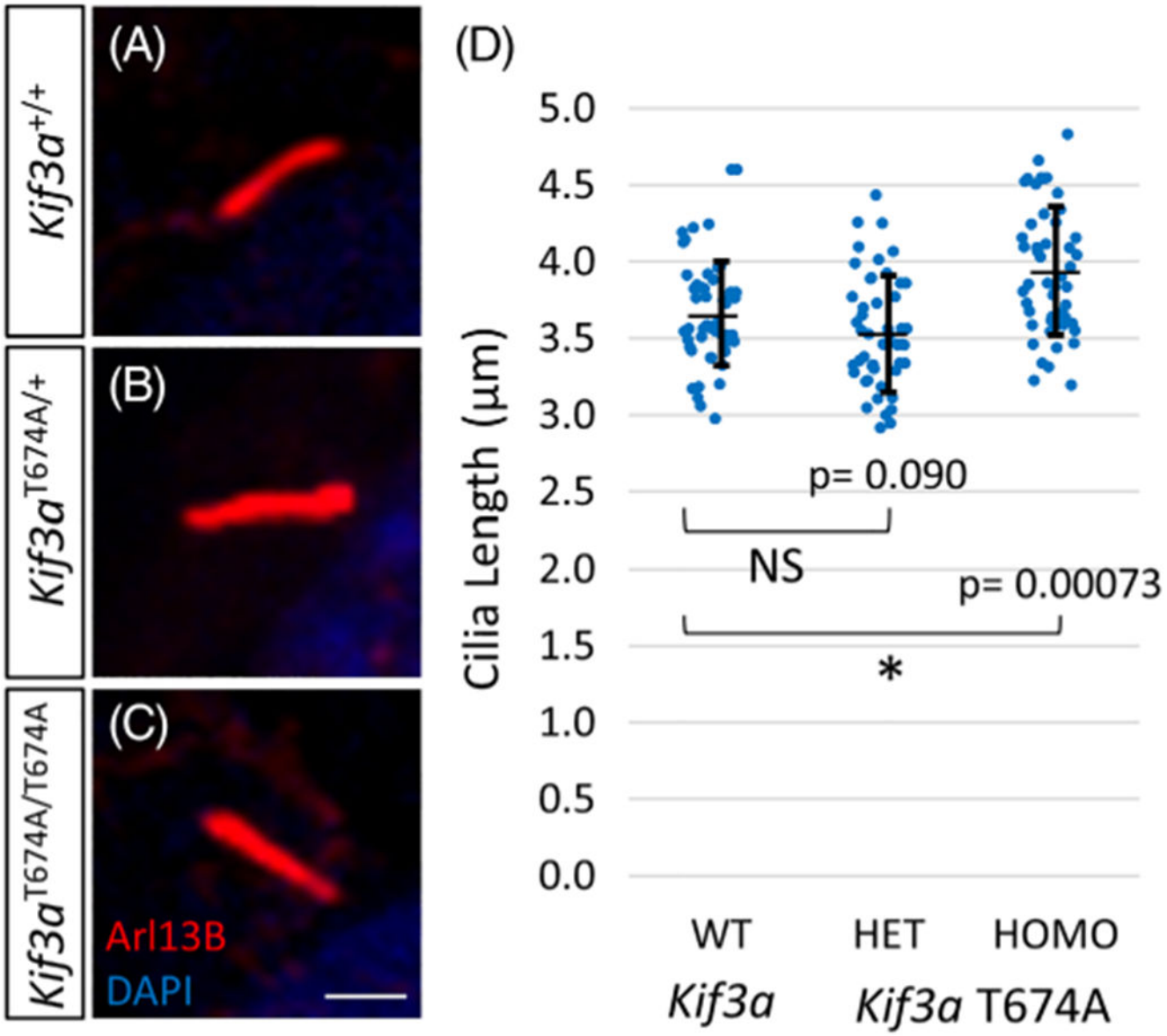

FIGURE 6.

Kif3a T674A homozygous mutant cells show a moderate increase in cilia length. A-C, Confocal immunofluorescence images show primary cilia (Arl13B, red) and nucleus (DAPI, blue) in Kif3a WT and T674A mutant mouse embryonic fibroblasts. Scale bar, 2 µm. D, Measurement of cilia length in Kif3a WT and T674A heterozygous and homozygous mutant cells. Shown are average ± SD, n = 45 cilia per genotype, **P* < .05, NS = not significant

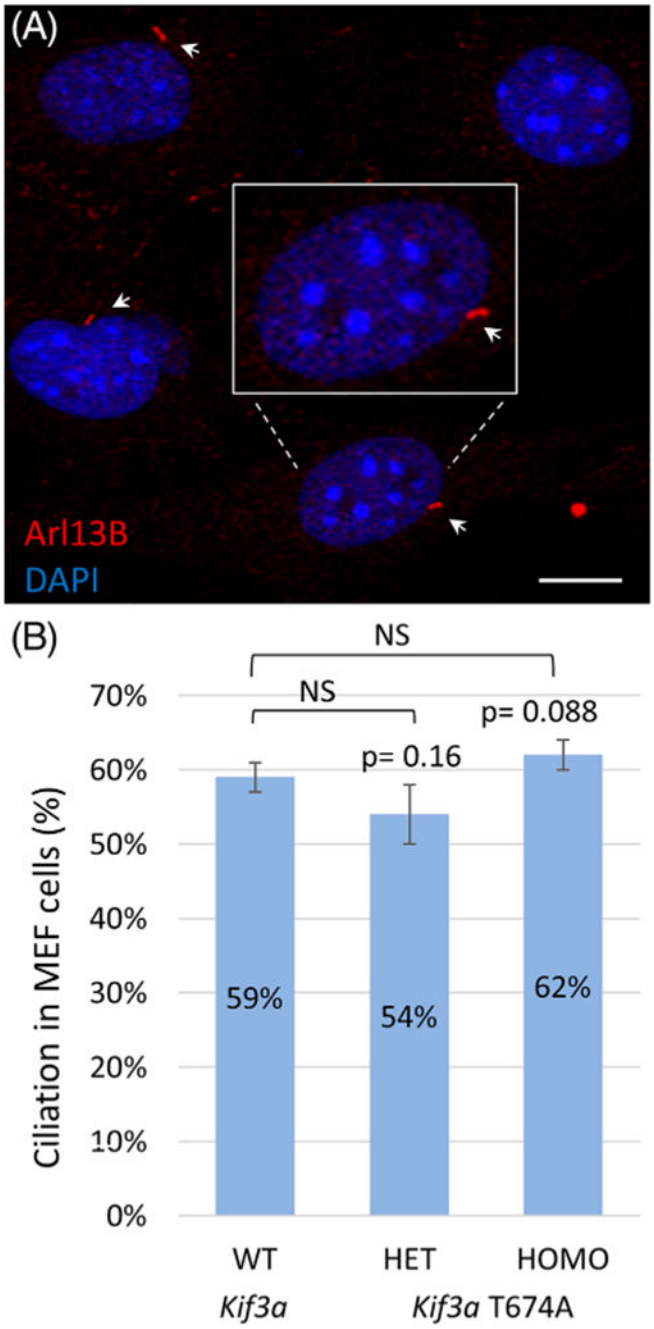

FIGURE 7.

Kif3a T674A mutant cells show insignificant change in the percent of ciliation. (A) A representative confocal immunofluorescence image shows ciliated vs nonciliated mouse embryonic fibroblasts. Primary cilia are labelled by Arl13B (red, arrow), and nucleus by DAPI (blue). Scale bar, 10 μm. (B) Measurement of percent of ciliation in Kif3a WT and T674A heterozygous (HET) and homozygous (HOMO) mutant cells. Shown are average ± SD, n = 140 cells per genotype, NS = not significant

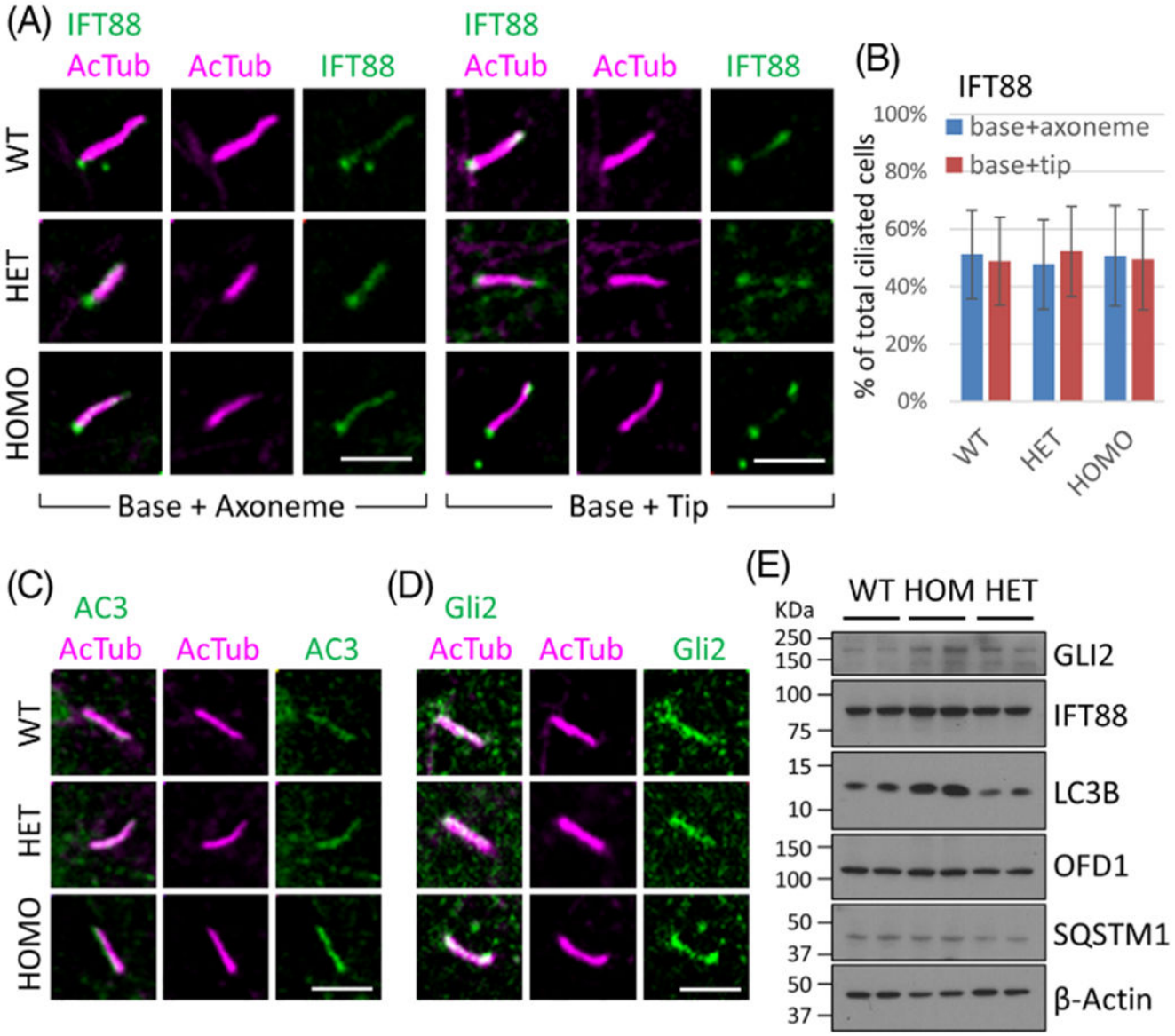

FIGURE 8.

Distribution and expression patterns of cilia and autophagy markers in Kif3a wild type and T674A mutant cells. Confocal immunofluorescence images illustrate ciliary localization of IFT88 (A), AC3 (C), and GLI2 (D) , in Kif3a WT and T674A mutant mouse embryonic fibroblasts. Scale bar, 3 μm. The percent of two IFT88 ciliary localization patterns between different *Kif3a* genotypes is shown as average ± SD in (B). Western blots show expression patterns of cilia (IFT-88 and GLI2) and autophagy markers (LC3B, OFD1, and SQSTM1) in Kif3a WT and T674A mutant mouse embryonic fibroblasts, (E). Beta-Actin signals indicate equal loading to total proteins from whole cell lysates